Sea surface height evidence for long-term warming effects of tropical cyclones on the ocean

Wei Mei[a,1], François Primeau[a], James C. McWilliams[b], and Claudia Pasquero[c]

[a]Department of Earth System Science, University of California, Irvine, CA 92697; [b]Department of Atmospheric and Oceanic Sciences, University of California, Los Angeles, CA 90095; and [c]Department of Earth and Environmental Sciences, University of Milan-Bicocca, I-20126 Milan, Italy

Edited by Kerry A. Emanuel, Massachusetts Institute of Technology, Cambridge, MA, and approved July 16, 2013 (received for review April 9, 2013)

Tropical cyclones have been hypothesized to influence climate by pumping heat into the ocean, but a direct measure of this warming effect is still lacking. We quantified cyclone-induced ocean warming by directly monitoring the thermal expansion of water in the wake of cyclones, using satellite-based sea surface height data that provide a unique way of tracking the changes in ocean heat content on seasonal and longer timescales. We find that the long-term effect of cyclones is to warm the ocean at a rate of 0.32 ± 0.15 PW between 1993 and 2009, i.e., ∼23 times more efficiently per unit area than the background equatorial warming, making cyclones potentially important modulators of the climate by affecting heat transport in the ocean–atmosphere system. Furthermore, our analysis reveals that the rate of warming increases with cyclone intensity. This, together with a predicted shift in the distribution of cyclones toward higher intensities as climate warms, suggests the ocean will get even warmer, possibly leading to a positive feedback.

Strong winds associated with tropical cyclones (TCs) increase air–sea heat fluxes, favoring the intensification of storms, and generate vigorous vertical mixing in the upper ocean, stirring warm surface waters with colder waters below (1–6). The wake produced by the passage of TCs is thus characterized by a surface cold anomaly and a subsurface warm anomaly (1–3, 6, 7). After the TC passage, the sea surface cold anomaly dissipates quickly (8–10), due in part to anomalous air–sea heat fluxes (9, 11), whereas the subsurface warm anomaly is believed to persist over a much longer period (12). This has led to the suggestion that the net long-term effect of TCs is to pump heat into the ocean (13–16). Such a flux of heat into the low-latitude ocean has been proposed to be an important modulator of local and remote climate (12, 17–22).

During the past decade or so, several studies have been devoted to estimating the magnitude of this heating effect, using sea surface temperature (SST) data (13–16). However, owing to a lack of subsurface temperature observations, these studies relied upon many assumptions that led to large and poorly quantified uncertainties (*SI Appendix*, *SI Results*). Furthermore, it is currently highly debated how much (if any) of the estimated warming survives beyond winter season when the deepening of the mixed layer cools the upper ocean. To avoid the ideological and methodological challenges inherent in the previous work, we take a more straightforward approach that was first proposed by Emanuel (13, 23) and quantify the TC-induced warming effect on the ocean by estimating the thermal expansion of water in the wake of Northern Hemisphere TCs, using satellite-derived sea surface height (SSH) data (24) together with tropical cyclone best-track data (25, 26). Combining these two datasets allows us to track the SSH anomalies (SSHAs) around the TC-generated wake beyond the winter season and thus provides a clear picture of the temporal evolution of the TC-induced changes in the ocean heat content. Details on the data and methods are given in *SI Appendix*, *SI Data and Methods*.

Results

Fig. 1 and *SI Appendix*, Fig. S1 show the temporal evolution of the along-track-averaged composite SSHA before and following the passage of a TC. Prominent negative SSHAs near the storm center are due to divergent Ekman flow induced by the cyclonic wind stress during the passage of the storm (27) and also to the evaporative enthalpy loss. Farther away from the storm center, the wind stress curl drives convergent Ekman transport and positive SSHAs; the anomalies are larger on the right because of the stronger winds (and thus wind stress curl) to the right of the storm (1) (*SI Appendix*, Fig. S2). The fact that the magnitude of the SSHAs correlates with the storm intensity (*SI Appendix*, Fig. S1) is discussed later.

In the weeks following the passage of the TC, the induced SSHAs propagate to the left of the storm track, consistent with the westward propagation of the SST anomalies (SSTAs) (16, 28) due to an increase in the environmental rotation rate with latitude (29). The SSHAs also dissipate as the flow crosses the SSH isolines before the current comes into geostrophic balance and as air–sea heat fluxes warm the cold surface anomalies. For our purposes, the former effect needs to be removed because it masks steric adjustments that are the signature of the net TC-induced warming of the ocean. Because both Ekman transport and geostrophic adjustment redistribute water mass only in the horizontal direction, their effect can be minimized by averaging over a sufficiently large area. To achieve this, we average the along-track-mean composite SSHA over a 2,000-km-wide strip centered on the storm track (*SI Appendix*, *SI Data and Methods*). The evolution of the area-averaged SSHA can be attributed primarily to anomalous air–sea heat fluxes; significant mass fluxes due to precipitation occur only during the storm passage and have at most a minor effect, as demonstrated by the fact that the SSHA under the storm is negative (Fig. 1 and *SI Appendix*, Fig. S1), whereas a positive anomaly is expected from an analysis of the precipitation rate (*SI Appendix*, Fig. S3), assuming a spatially uniform evaporation rate and assuming the amount of water mass that radiates away by barotropic adjustment is negligible (30).

The area-mean SSH for cyclones of tropical storm intensity and above shows a pronounced reduction concurrent with the storm passage, as expected because of the enhanced air–sea heat losses (red line in Fig. 2). Note that the magnitude of the negative SSHA should be considered a lower bound and not a direct estimate of the sea level drop, as heavy rains associated with the passage of the storm have a detrimental effect on altimeter measurements (31). Subsequently, the temporal evolution shows a rapid SSH increase during the first month, followed by a more gradual increment that levels off after about 5 mo. This behavior is consistent with recent observations showing that the warming by anomalous air–sea heat fluxes is initially confined to the top part of the mixed layer and is associated with a rapid recovery of

Author contributions: W.M. and C.P. designed research; W.M. performed research; F.P., J.C.M., and C.P. contributed new reagents/analytic tools; W.M. analyzed data; and W.M., F.P., J.C.M., and C.P. wrote the paper.

The authors declare no conflict of interest.

This article is a PNAS Direct Submission.

[1]To whom correspondence should be addressed. E-mail: wmei@ucsd.edu.

This article contains supporting information online at www.pnas.org/lookup/suppl/doi:10.1073/pnas.1306753110/-/DCSupplemental.

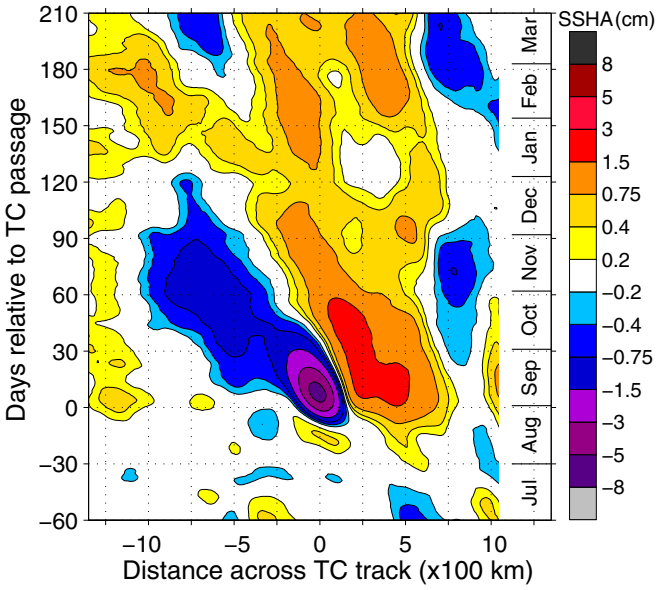

Fig. 1. Temporal evolution of along-track–averaged composite SSHA (centimeters) associated with the passage of TCs of category-3 to -5 hurricane intensity in the Northern Hemisphere. To provide a general sense of a rough timeline, the averaged calendar date corresponding to the time on the left *y* axis is shown on the right *y* axis. For example, the mean occurrence calendar date of category-3 to -5 hurricanes is around the end of August; an individual category-3 to -5 hurricane, however, may occur anytime during the TC season, which usually lasts for 6 mo or longer.

the SST within a few weeks (8–10), whereas the bottom part of the TC-induced cold anomaly takes a much longer period to dissipate (32, 33) (see also a scaling argument discussed in *SI Appendix*, *SI Results*).

To quantify the long-term change in ocean heat content induced by TCs we use the SSHA averaged over a window that covers the quasi-steady stage in the period between 5 mo and 7 mo after the storm passage. This period is sufficiently long that the averaging window extends beyond the period of deepest winter mixed layer (*SI Appendix*, Fig. S4), thus ensuring that our estimate filters out short-term heating that does not survive beyond the winter season (16). At the same time, the averaging period is sufficiently near in time to the passage of the storm to minimize the amount of heat lost by large-scale horizontal advection. We find that during this time period the sea level averaged over the 2,000-km length in the across-track direction is on average 0.21 ± 0.10 cm higher than during the prestorm period (Fig. 3, red dashed line).

To convert the SSHA (Δh) to the ocean heat uptake per unit length of the TC track (dQ/dx) we use $(dQ/dx)/\Delta h = 4\times10^{17}$ J·km^{-1}·cm^{-1} (*Materials and Methods*). By integrating over the mean length of TC tracks during a year using the 6-h TC best-track data (*SI Appendix*, *SI Data and Methods*), we get the annual cumulative warming effect induced by TCs globally as 1.01 ± 0.46 × 10^{22} J. This corresponds to a mean ocean heat uptake rate of 0.32 ± 0.15 PW, which is within the range given by previous studies (i.e., 0.15–1.5 PW) (13–16) and is approximately two times the most recent estimate (16). Calculations based on early- or late-season TCs give a similar estimate of the long-term effect (*SI Appendix*, Fig. S5).

When the above analysis is conditioned on TC intensity, we find that the magnitude of the local SSHA correlates with the storm strength. For category-3 to -5 hurricanes the maximum amplitude of the negative local SSHA is on average 6 cm, whereas the magnitude for tropical depressions is only 1.5 cm (*SI Appendix*, Fig. S1). The temporal evolution of the area-averaged composite SSHA is shown in Fig. 2 for different intensity classes. After the rapid increase of SSH in the first month after the passage of the storm, found for all intensity groups, the SSHA associated with tropical depressions changes very little whereas that associated with stronger TCs keeps increasing. We interpret this as evidence that the cold SSTA in the wake of the tropical depressions has already completely disappeared by day 30, thus shutting off the anomalous air–sea heat fluxes, whereas the SST in the wake of stronger TCs is still below normal conditions, allowing anomalous air–sea heat fluxes to continue warming the ocean (28). The remaining negative SSHA associated with tropical depressions is eliminated during the winter season when the mixed-layer depth increases beyond the maximum depth of the subsurface cold anomaly. For stronger storms, the anomaly remains positive after the winter mixed-layer deepening, indicating that part of the anomalous warming lies below the winter mixed-layer depth. On long timescales tropical depressions have little or no effect on ocean heat uptake, but stronger TCs produce a significant net ocean heating. The heating effect is particularly strong for category-3 to -5 hurricanes with an ocean warming of 1.56 ± 0.90 × 10^{17} J·km^{-1} whereas for tropical storms it is only 0.63 ± 0.48 × 10^{17} J·km^{-1} (see Fig. 3 where the SSHA averaged over months 5–7 after the passage of the storm is shown together with the implied heat uptake).

Conclusion and Discussion

Taking advantage of the continuous measurements of SSH from space by satellite altimetry, we were able to track the temporal evolution of the TC-generated changes in the ocean heat content. The long-term warming effect induced by global TCs on the ocean is estimated to be 1.01 ± 0.46 × 10^{22} J on a yearly basis over the study period between 1993 and 2009. A better feel for such a TC-induced warming effect can be achieved when we divide it by the total annual area affected by TCs (on average ~9 × 10^{13} m^2) and by the averaged duration of TC winds at each

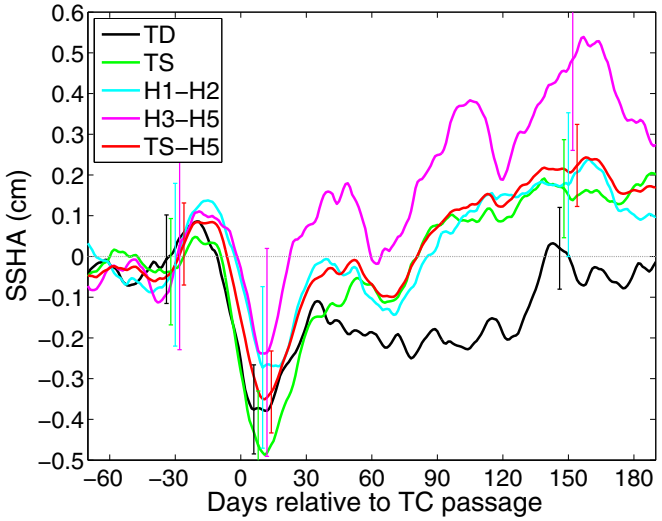

Fig. 2. Temporal evolution of area-averaged composite SSHA associated with the passage of TCs of different intensity in the Northern Hemisphere: tropical depressions (black), tropical storms (green), category-1 to -2 hurricanes (light blue), category-3 to -5 hurricanes (magenta), and all cyclones of tropical storm intensity and above (red). Error bars are calculated as the SD divided by the square root of the number of independent observations (i.e., the SEM) and are shown for days −30, 10, and 150. For each given intensity group, the number of independent observations for a given storm track is approximated as the number of observations that are separated by the spatial decorrelation scale estimated to be ~200 km (*SI Appendix*, Fig. S7), and the observations from different storms are assumed independent.

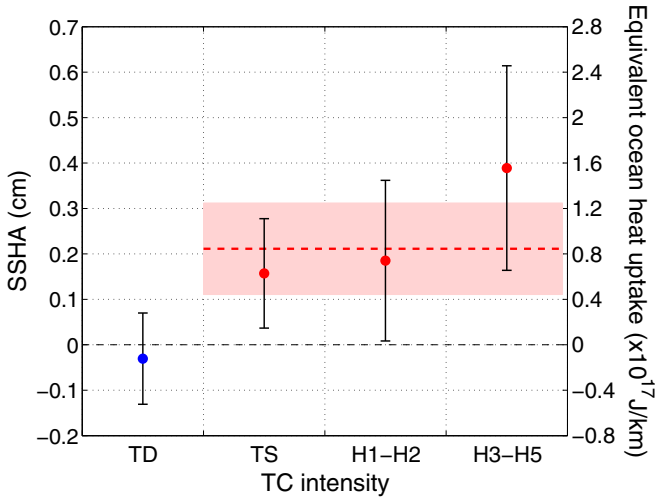

Fig. 3. SSHA associated with the passage of TCs of different intensity in the Northern Hemisphere averaged during the period of maximum mixed-layer depth in the winter season. The mean value for all cyclones of tropical storm intensity and above is denoted as the red dashed horizontal line with the pink shading showing the error bar. The averaging period is from day 135 to day 175 (Fig. 2) for tropical depressions, tropical storms, category-1 to -2 hurricanes, and all cyclones of tropical storm intensity and above and from day 120 to day 190 for category-3 to -5 hurricanes. (The reason for using a different averaging window for category-3 to -5 hurricanes is that the subseasonal oscillation is very large for this group of TCs.) Error bars are calculated in the same way as in Fig. 2. The equivalent ocean heat uptake is expressed as the warming per unit length along the TC track, and it is calculated using Eq. **1** in *Materials and Methods*.

location (~1.4 d); the obtained warming rate is O(900 W·m^{-2}), which is ~23 times larger than the background warming rate over the equatorial area where the background warming is the most intense (~40 W·m^{-2}; calculated using National Centers for Environmental Prediction/National Center for Atmospheric Research reanalysis data) (34). Expressed as the spatially integrated forcing, the TC-induced mean ocean heat uptake rate of 0.32 ± 0.15 PW is comparable to ~15% of the peak global ocean heat transport (35), as already discussed in previous studies (e.g., ref. 14). These comparisons suggest that TCs are very efficient agents of ocean warming and thus play an important part in the climate system.

In addition, it is worth noting that part of the TC-induced anomalous heat in the upper ocean is released to the atmosphere from the ocean during the winter season because of the deepening of the seasonal mixed layer (36). The resultant anomalous heating of the winter tropical and subtropical atmosphere may influence the climate by enhancing the poleward heat transport in the atmosphere. This effect, not considered in our estimates, represents another aspect of the active role of TCs in the climate system.

Stratified by TC intensity, our analysis further shows that the amplitude of the long-term warming effect strongly depends on TC intensity: TCs of tropical depression intensity have little or no effect on the ocean heat budget whereas stronger TCs significantly warm the ocean. To elucidate the processes responsible for the dependence of the net long-term heating on TC intensity we consider three possible situations illustrated in Fig. 4 and *SI Appendix*, Fig. S6, i.e., no effect, net cooling, and net warming: (*i*) The no-effect case occurs if the TC-induced mixing-layer depth (h_{tc}) is shallower than the depth of the climatological winter mixed layer (h_w); then the imprint of the TC is completely erased by the seasonal evolution of the climatological mixed layer. This case is more likely to occur for weak storms. (*ii*) The net-cooling case is possible for weak storms if the cooling below h_w is stronger than the warming at greater depths. This situation is possible for storms that occur over the region where the difference between h_w and the climatological summer mixed-layer depth h_s is small, such as within the latitude band equatorward of ~10° (see *SI Appendix*, *SI Results* for a more detailed discussion). (*iii*) The net-warming case occurs for strong storms where h_{tc} reaches below h_w so that a significant amount of warming can survive beyond the winter season. Generally, the fraction of the warming increases as h_{tc} increases and thus we expect to see stronger TCs lead to a stronger warming effect. The three possible cases are also summarized in a regime diagram of TC-induced SST and mixing-layer depth, (T_{tc}, h_{tc}), in *SI Appendix*, *SI Results*.

Recent studies (37–41) either predict or suggest that in the near future the frequency of intense TCs, particularly category-3 to -5 hurricanes, will increase in response to warming climate. This together with the extremely high efficiency of these intense

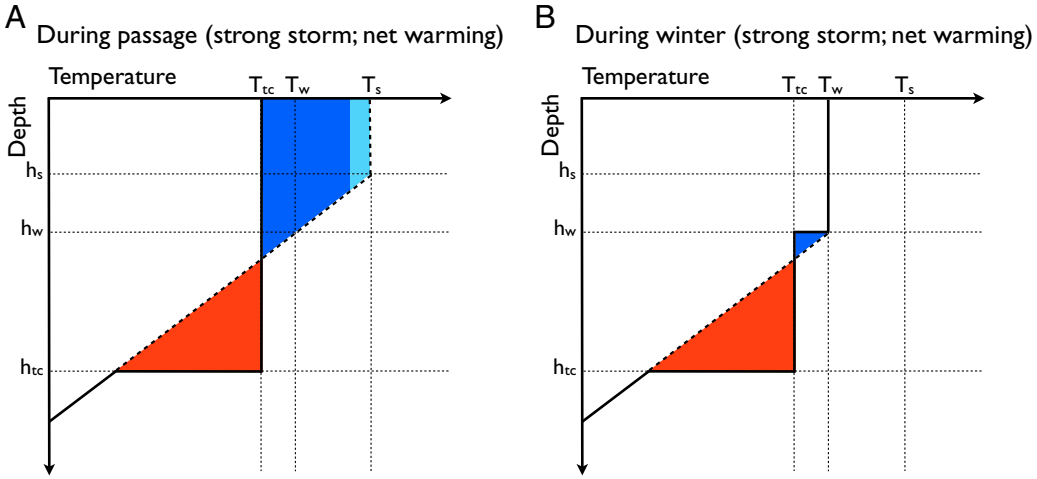

Fig. 4. (*A* and *B*) Schematic diagram for the change in the vertical temperature profile for the case of strong storms with net warming: (*A*) immediately after the TC passage and (*B*) after the winter season. Dashed lines show the climatological condition, and solid lines show the situation with the effect of the TC. Red and blue colors indicate, respectively, warming and cooling with respect to climatological conditions. Light blue shows the heat extracted from the ocean during the passage of the storm. h_s, climatological mixed-layer depth during the summer season; h_{tc}, TC-induced mixing-layer depth; h_w, climatological mixed-layer depth during the winter season; T_s, climatological SST during the summer season; T_{tc}, minimum SST after the TC passage; T_w, climatological SST during the winter season. (See *SI Appendix*, Fig. S6 for the cases with weak storms that lead to either net cooling or no effect.)

TCs at heating the ocean should accelerate the warming of the oceans, which in turn should feed back positively on TC activity. Furthermore, analyses of output from models participating in the fifth phase of the Coupled Model Intercomparison Project (42) suggest that for most of the TC-active region, the ocean mixed layer gets shallower in the winter season whereas it changes little during the TC-active season under global warming (*SI Appendix*, *SI Results*). This projected change would allow more TC-pumped heat to persist in the permanent thermocline, potentially making the feedback between TC activity and ocean warming even stronger.

Materials and Methods

In this section, we provide a summary of the methodology in use; more detailed description of the data and methods can be found in *SI Appendix, SI Data and Methods*. We used SSH data from Archiving, Validation, and Interpretation of Satellite Oceanographic gridded fields and computed the SSHAs after removing the climatological seasonal cycle, the long-term linear trend, and the variability associated with the El Niño/Southern Oscillation. For each 6-h best-track storm location we defined a domain centered on the storm center with size 3,000 km along the direction perpendicular to the storm track and ~144 km along the track and constructed a grid within the domain with a resolution of ~12 km × 12 km. The SSHAs were then linearly interpolated onto the grids of the newly constructed domain, resulting in a spatial map of SSHA for each storm location and each analyzed day. These maps were composited based on the date with respect to the time of the storm passage and on the storm intensity, and the composite analysis was performed from about 2 mo before the storm passage and until 7 mo after it, to characterize the spatial structure of the SSH left behind TCs and examine its temporal evolution. The results shown were averages in the along-track direction (Fig. 1) or averages in both the along-track and across-track directions (Figs. 2 and 3).

To convert SSHA (Δh) to ocean heat uptake per unit length of the TC track (dQ/dx) we use $(dQ/dx)/\Delta h = 4\times10^{17}\ \mathrm{J\cdot km^{-1}\cdot cm^{-1}}$ obtained from the relationship

$$\frac{dQ}{dx} = \frac{\rho_0 c_p \Delta h L}{\alpha}, \qquad [1]$$

where $\rho_0 = 1,000\ \mathrm{kg\cdot m^{-3}}$ is the reference seawater density, $c_p = 4\times10^3\ \mathrm{J\cdot kg^{-1}}$ is the specific heat of seawater, L = 2,000 km is the cross-track distance over which the average is performed, and $\alpha = 2\times10^{-4}\ \mathrm{K^{-1}}$ is the thermal expansion coefficient.

The annual cumulative warming effect induced by TCs globally is calculated via $Q = U\cdot\Delta t\cdot[(dQ/dx)_{\mathrm{TS}}\,N_{\mathrm{TS}} + (dQ/dx)_{\mathrm{H1-H2}}\,N_{\mathrm{H1-H2}} + (dQ/dx)_{\mathrm{H3-H5}}\,N_{\mathrm{H3-H5}}]$, with N the recorded mean annual number of observations at 6-h intervals (only one observation is counted if the distance between two observations that are located along two different TC tracks is shorter than 200 km and the separation between their occurrence is shorter than 5 mo); U = 5 $\mathrm{m\cdot s^{-1}}$ the mean translation speed of a storm; $\Delta t = 6$ h the time interval of the observations in best-track data; and the subscripts "TS", "H1–H2", and "H3–H5", respectively, representing tropical storm, category-1 to -2 hurricane, and category-3 to -5 hurricane. The ocean heat uptake rate is computed by dividing the annual warming effect by 1 y: $\mathrm{OHU} = Q/t$ with $t = 365\times86,400$ s.

ACKNOWLEDGMENTS. We thank Prof. Robert Korty, an anonymous reviewer, and the editor for their insightful and constructive comments that helped us to improve the manuscript. We also thank Prof. Kerry Emanuel for sharing the compiled tropical cyclone best-track data. This work was funded by the National Aeronautics and Space Administration (NASA) Headquarters under the NASA Earth and Space Science Fellowship Program, Grant NNX10AP30H. W.M. and F.P. also acknowledge support from National Science Foundation Grant OCE-0928395. C.P. was partially funded by the Flagship Project RITMARE – The Italian Research for the Sea – funded by the Italian Ministry of Education, University, and Research within the National Research Program 2011-2013. The altimeter products were produced by Ssalto/Duacs and distributed by Archiving, Validation, and Interpretation of Satellite Oceanographic data (AVISO) with support from the Centre National d'Études Spatiales (CNES).

1. Price JF (1981) Upper ocean response to a hurricane. *J Phys Oceanogr* 11(2):153–175.
2. Ginis I (2002) Tropical cyclone-ocean interactions. *Atmosphere-Ocean Interactions*, Advances in Fluid Mechanics Series, ed Perrie W (WIT Press, Southampton, UK), Vol 33, pp 83–114.
3. Zedler SE, et al. (2002) Analysis and simulations of the upper ocean's response to Hurricane Felix at the Bermuda Testbed Mooring site: 13-23 August 1995. *J Geophys Res* 107(C12):3232, 10.1029/2001JC000969.
4. Black PG, et al. (2007) Air-sea exchange in hurricanes: Synthesis of observations from the coupled boundary layer air-sea transfer experiment. *Bull Am Meteorol Soc* 88(3):357–374.
5. Sanford TB, Price JF, Girton JB (2011) Upper-ocean response to Hurricane Frances (2004) observed by profiling EM-APEX floats. *J Phys Oceanogr* 41(6):1041–1056.
6. Vincent EM, et al. (2012) Processes setting the characteristics of sea surface cooling induced by tropical cyclones. *J Geophys Res* 117(C2):C02020.
7. Wentz FJ, Gentemann C, Smith D, Chelton D (2000) Satellite measurements of sea surface temperature through clouds. *Science* 288(5467):847–850.
8. Hart RE, Maue RN, Watson MC (2007) Estimating local memory of tropical cyclones through MPI anomaly evolution. *Mon Weather Rev* 135(12):3990–4005.
9. Price JF, Morzel J, Niiler PP (2008) Warming of SST in the cool wake of a moving hurricane. *J Geophys Res* 113(C7):C07010.
10. Dare RA, McBride JL (2011) Sea surface temperature response to tropical cyclones. *Mon Weather Rev* 139(12):3798–3808.
11. Mei W, Pasquero C (2012) Restratification of the upper ocean after the passage of a tropical cyclone: A numerical study. *J Phys Oceanogr* 42(9):1377–1401.
12. Pasquero C, Emanuel K (2008) Tropical cyclones and transient upper-ocean warming. *J Clim* 21(1):149–162.
13. Emanuel K (2001) Contribution of tropical cyclone to meridional heat transport by the oceans. *J Geophys Res* 106(D14):14771–14781.
14. Sriver RL, Huber M (2007) Observational evidence for an ocean heat pump induced by tropical cyclones. *Nature* 447(7144):577–580.
15. Sriver RL, Huber M, Nusbaumer J (2008) Investigating tropical cyclone-climate feedbacks using the TRMM Microwave Imager and the Quick Scatterometer. *Geochem Geophys Geosyst* 9(9):Q09V11.
16. Jansen M, Ferrari R, Mooring TA (2010) Seasonal versus permanent thermocline warming by tropical cyclones. *Geophys Res Lett* 37(3):L03602.
17. Emanuel K (2002) A simple model of multiple climate regimes. *J Geophys Res* 107(D9): 4077, 10.1029/2001JD001002.
18. Korty RL, Emanuel KA, Scott JR (2008) Tropical cyclone-induced upper-ocean mixing and climate: Application to equable climates. *J Clim* 21(4):638–654.
19. Jansen M, Ferrari R (2009) Impact of the latitudinal distribution of tropical cyclones on ocean heat transport. *Geophys Res Lett* 36(6):L06604.
20. Fedorov AV, Brierley CM, Emanuel K (2010) Tropical cyclones and permanent El Niño in the early Pliocene epoch. *Nature* 463(7284):1066–1070.
21. Sriver RL, Goes M, Mann ME, Keller K (2010) Climate response to tropical cyclone-induced ocean mixing in an Earth system model of intermediate complexity. *J Geophys Res* 115(C10):C10042.
22. Scoccimarro E, et al. (2011) Effects of tropical cyclones on ocean heat transport in a high-resolution coupled general circulation model. *J Clim* 24(16):4368–4384.
23. Emanuel K (2008) The hurricane-climate connection. *Bull Am Meteorol Soc* 89(5):ES10–ES20.
24. Ducet N, Le Traon PY, Reverdin G (2000) Global high-resolution mapping of ocean circulation from TOPEX/Poseidon and ERS-1 and -2. *J Geophys Res* 105(C8):19477–19498.
25. Chu J-H, Sampson CR, Levine AS, Fukada E (2002) *The Joint Typhoon Warning Center Tropical Cyclone Best-Tracks, 1945–2000, Ref NRL/MR/7540-02-16* (Naval Research Laboratory, Washington, DC).
26. McAdie CJ, et al. (2009) *Tropical Cyclones of the North Atlantic Ocean, 1851–2006*, Historical Climatology Series 6-2 (National Climatic Data Center, Asheville, NC, in cooperation with the National Hurricane Center, Miami).
27. Shay LK, Chang SW (1997) Free surface effects on the near-inertial ocean current response to a hurricane: A revisit. *J Phys Oceanogr* 27(1):23–39.
28. Mei W, Pasquero C (2013) Spatial and temporal characterization of sea surface temperature response to tropical cyclones. *J Clim* 26(11):3745–3765.
29. McWilliams JC, Flierl GR (1979) On the evolution of isolated, nonlinear vortices. *J Phys Oceanogr* 9(6):1155–1182.
30. Huang RX, Jin X (2002) Sea surface elevation and bottom pressure anomalies due to thermohaline forcing. Part I: Isolated perturbations. *J Phys Oceanogr* 32(7):2131–2150.
31. Carrère L, Mertz F, Dorandeu J, Quilfen Y, Patoux J (2009) Observing and studying extreme low pressure events with altimetry. *Sensors* 9(3):1306–1329.
32. D'Asaro E, et al. (2011) Typhoon-ocean interaction in the western North Pacific: Part 1. *Oceanography* 24(4):24–31.
33. Park JJ, Kwon Y-O, Price JF (2011) Argo array observation of ocean heat content changes induced by tropical cyclones in the north Pacific. *J Geophys Res* 116(C12):C12025.
34. Kalnay E, et al. (1996) The NCEP/NCAR 40-year reanalysis project. *Bull Am Meteorol Soc* 77(3):437–471.
35. Ganachaud A, Wunsch C (2003) Large-scale ocean heat and freshwater transports during the World Ocean Circulation Experiment. *J Clim* 16(4):696–705.
36. Vincent EM, et al. (2012) Influence of tropical cyclones on sea surface temperature seasonal cycle and ocean heat transport. *Clim Dyn*, 10.1007/s00382-012-1556-0.
37. Elsner JB, Kossin JP, Jagger TH (2008) The increasing intensity of the strongest tropical cyclones. *Nature* 455(7209):92–95.
38. Emanuel K, Sundararajan R, Williams J (2008) Hurricanes and global warming: Results from downscaling IPCC AR4 simulations. *Bull Am Meteorol Soc* 89(3):347–367.
39. Bender MA, et al. (2010) Modeled impact of anthropogenic warming on the frequency of intense Atlantic hurricanes. *Science* 327(5964):454–458.
40. Knutson TR, et al. (2010) Tropical cyclones and climate change. *Nat Geosci* 3(3):157–163.
41. Murakami H, et al. (2012) Future changes in tropical cyclone activity projected by the new high-resolution MRI-AGCM. *J Clim* 25(9):3237–3260.
42. Taylor KE, Stouffer RJ, Meehl GA (2012) An overview of CMIP5 and the experiment design. *Bull Am Meteorol Soc* 93(4):485–498.